Unified Description of Proton NMR Relaxation in Water, Acetonitrile, and Methane from Molecular Dynamics Simulations in the Liquid, Supercritical and Gas Phases

Adam Philips^a, Jochen Autschbach^{a,*}

Department of Chemistry
 University at Buffalo

 State University of New York
 Buffalo, NY 14260-3000, USA

 email: jochena@buffalo.edu

Dec 28, 2022

Abstract

A comprehensive calculation of proton NMR relaxation in water, acetonitrile, and methane across a wide range of the phase diagram, is provided via ab initio and force field-based molecular dynamics simulations. The formalism used for the spin-rotation (SR) contribution to relaxation is developed for use with any molecular symmetry and utilizes the full molecular SR tensors, which are calculated from first principles via Kohn-Sham (KS) DFT. In combination with calculations of the dipolar contribution, near quantitative agreement with total measured relaxation rates is achieved.

1 Introduction

For protons in small-molecule liquids and gasses, the most prominent NMR relaxation mechanisms are fluctuating dipolar interactions, and spin-rotation (SR) interactions. The former are both intraand intermolecular in nature; driven by dipole-dipole interactions between nuclear spins in the same molecule versus neighboring ones, and modulated by molecular translation, rotation, and vibration. The SR mechanism is essentially purely intramolecular and results from the interactions of nuclear spins with the fluctuating local magnetic fields generated by molecular rotation. The present work continues our efforts^{1–5} to calculate NMR relaxation properties accurately by applying first principles methods via Kohn-Sham density functional theory (KS DFT) to the simulation of dynamics, and where applicable, to the calculation of interaction tensors such as electric field gradients and SR tensors. This first principles approach allows for detailed insight into the microscopic dynamics that drive key mechanisms of nuclear spin relaxation and provides a technique that is—in principle—generalizable to systems containing elements from across the periodic table without the need for empirical parameters or force fields. For example, we previously applied our work on quadrupolar relaxation to an exotic chemical system containing a sodide anion, and were able to rationalize its seemingly 'genuine' gas phase ion behavior in NMR experiments from a first principles perspective.^{6,7}

The simple molecular systems chosen for this study have a long history in the NMR relaxation literature. Methane is the canonical example of the spherical top molecule, while acetonitrile and water are commonly chosen representatives for symmetric and asymmetric tops, respectively. NMR relaxation has a vast range of applications. Among them, magnetic resonance imaging is well known. More exotic applications include ¹H NMR relaxation measurements of methane in the characterization of crude oil.^{8–10}

In a series of recent papers, ^{11–14} Singer et al. used classical dynamics to study the dipolar and SR contributions to ¹H relaxation in various hydrocarbons. In 2018, the group studied methane at various temperatures and pressures. ¹² A major result of their work was the development of an empirical description of relaxation as a function of self-diffusion coefficients in the supercritical region. We refer to the Singer et al. results throughout this work, to benchmark our calculations for methane as well as validate our implementation of the theory (see the following section). ¹H relaxation in acetonitrile and its relevant dynamic properties have been studied extensively experimentally, ^{15–17} and theoretically by Gerig et al., ¹⁸ among others. ^{19,20} Acetonitrile is expected to have roughly equal contributions from the dipolar and SR mechanisms at ambient conditions. ¹⁵ In contrast, water has no appreciable SR contribution in the liquid phase but the mechanism has recently been shown to be dominant in vapor phase measurements by Mammoli et al., Ref. 21. In light of the results from Ref. 21, we developed a set of force field-based gas phase water simulations, matching pressure and temperature conditions, to reproduce from theory the experimentally measured longitudinal relaxation rates with high accuracy.

The current work is laid out as follows. In Section 2, an overview of the theoretical formalism describing SR relaxation is provided, which summarizes the hierarchy of approximations that lead to the theory implemented in this work. Also provided is a summary of the computational details for MD simulations and calculation of molecular SR tensors. Details about our implementation for dipolar relaxation were given previously in Ref. 4 and are therefore not discussed herein. In Section 4, the primary results of the SR and dipolar relaxation rate calculations are reported and discussed in terms of their accuracy with respect to experimental and other theoretical results, as well as in terms of the dynamical features in the MD that lead to the obtained results. Section 5 provides a brief summary and conclusions.

2 Theory

The theory of NMR relaxation was pioneered by Bloembergen, Purcell, and Pound, ²² Redfield, ²³ Bloch, ²⁴ and others. ^{25,26} The SR mechanism is described in detail in References 27–32. References 33–36 give special attention to the SR mechanism in the gas phase. The theoretical framework which allows for the determination of quadrupolar and dipolar NMR relaxation rates from molecular dynamics simulations is layed out in various pioneering articles ^{37–42} and in our previous work. ^{2–4} A cursory overview of the SR mechanism was also provided in Ref. 4 along with an estimate of its role in ¹H relaxation in liquid acetonitrile. The approximations employed in that work were crude, in part, because they did not require explicit calculation of molecular angular momentum correlation functions. Additionally,

the formulae used were derived exclusively for a spherical top molecule. A more complete description of SR relaxation is provided here and implemented in all subsequent calculations of total ¹H relaxation rates from MD simulations. The notation used herein follows Spiess.²⁶

SR relaxation is driven by the interaction of a nuclear spin with the magnetic field generated by the rotation of electric charges in its host molecule. In the principal axis frame of the moment of inertia of a given molecule, the spin interaction Hamiltonian for the SR mechanism is written as

$$\mathcal{H}_{SR} = \sum_{m=-1}^{1} (-1)^m I_m A_{-m} \tag{1}$$

where I_m are components of the nuclear spin operator. The A_m are composed of the characteristic spin-rotation tensor (with Cartesian elements, c_{ij}) and molecular angular momentum components J_j according to the following definitions

$$A_i = \sum_{j=x,y,z} c_{ij} J_j, \ i = x, y, z$$
 (2a)

$$A_{\pm 1} = \mp \frac{1}{\sqrt{2}} (A_x \pm i A_y), \ A_0 = A_z$$
 (2b)

The components of the molecular angular momentum are defined in the usual way as

$$J_i = \sum_j I_{ij} \omega_j \tag{3}$$

where ω is the vector describing the molecular angular velocity and I_{ij} is an element of the molecular moment of inertia tensor I. A_m also contain the time-dependence of the interaction as a result of fluctuations of molecular angular momentum. A master equation for the relaxation phenomenon takes the form of a differential equation of motion of the density operator, ρ , describing the quantum state of an ensemble of spins. In the rotating frame, indicated by ρ^* , this master equation is written as

$$\frac{d\rho^*}{dt} = -\sum_{m_1=-1}^{1} \sum_{m_2=-1}^{1} (-1)^{m_1+m_2} \sum_{m'=-1}^{1} [I_{m'}, [I_{-m'}, \rho^*]]
\cdot \int_{0}^{\infty} \langle \mathcal{D}_{-m',m_1}^{(1)} [-\Omega(t)] \mathcal{D}_{m',m_2}^{(1)} [-\Omega(t+\tau)] A_{m_1}(t) A_{m_2}(t+\tau) \rangle e^{im'\omega\tau} d\tau$$
(4)

The square brackets in the first line of Equation (4) indicate a nested commutator. $\mathcal{D}_{m',m}^{(1)}[-\Omega(t)]$ are elements of the the rank 1 Wigner rotation matrices applied to the orientational (Euler) angles of a molecule-fixed axis system.

Equation (4) contains half-Fourier transforms of coupled time autocorrelation functions of $\mathcal{D}_{m',m}^{(1)}$ and A_m , where τ is a delay time and $\langle ... \rangle$ indicates an average over the ensemble and time origins, t. With regard to this correlation function, a common approximation is made for systems in which molecular orientation and angular momentum are uncorrelated with one another. In this case, the

correlation functions can be decoupled as

$$\langle \mathcal{D}_{-m',m_{1}}^{(1)}[-\Omega(t)]\mathcal{D}_{m',m_{2}}^{(1)}[-\Omega(t+\tau)]A_{m_{1}}(t)A_{m_{2}}(t+\tau)\rangle$$

$$\simeq \langle \mathcal{D}_{-m',m_{1}}^{(1)}[-\Omega(t)]\mathcal{D}_{m',m_{2}}^{(1)}[-\Omega(t+\tau)]\rangle \langle A_{m_{1}}(t)A_{m_{2}}(t+\tau)\rangle$$
(5)

This simplification is known to be valid for isotropic liquids, however it is not expected to be generally valid in the case of low-density gasses, 29 as we confirm later in Section 4 by direct analysis of liquid and gas phase water simulations. Furthermore, for liquids the molecular orientation has a much longer correlation time than the angular momentum. Therefore, for a time τ on the order of the latter, the orientation at $t+\tau$ is essentially the same as at t. By applying properties of Wigner $\mathcal D$ matrices, this leads to the following simplification in which the dependence on the orientational correlation function is eliminated

$$\langle \mathcal{D}_{m',m_1}^{(1)}[-\Omega(t)]\mathcal{D}_{-m',m_2}^{(1)}[-\Omega(t+\tau)]\rangle \simeq \mathcal{D}_{m',m_1}^{(1)}[-\Omega(t)]\mathcal{D}_{-m',m_2}^{(1)}[-\Omega(t)]\rangle = (-1)^{m'+m_1}\frac{1}{3}\delta_{-m_1,m_2} \tag{6}$$

This approximation is considered valid for liquids and dense gasses. In low-density gasses, the molecular orientation is expected to decorrelate much faster due to long periods of free rotation during which the orientation is constantly changing in the laboratory frame. At the same time, the angular momentum is expected to decorrelate much more slowly as molecular collisions are comparatively rare. Explicit evaluation of the coupled correlation functions without the approximations of Equations (5) and (6) can be found in the literature in Refs. 43 and 29. The resulting expansion contains two terms which include contributions from the molecular orientation. One such term is proportional to the square of the 'diagonal' (anisotropic) SR coupling, $\Delta c = c_{zz} - c_{xx}$, and the other is a cross term proportional to the product of the average SR coupling, c_a , with Δc . In the unique case of water, the SR tensor is nearly isotropic, with our calculations giving principal components c_{xx} , c_{yy} , $c_{zz} = 36.9$, 33.5, 35.5 kHz. This results in a small coupling anisotropy, allowing the terms of the expanded correlation function containing contributions from orientational correlation to be neglected in a first approximation.

The approximations embodied by Equations (5) and (6) lead to the rate equations used by Singer et al.¹² for calculations of SR relaxation rates for methane. There, two unique rate equations were employed. An equation from Hubbard⁴³ makes the approximation of Equation (5) referred to as the "diffusion model", and an equation derived for spherical tops by Bloom et al.²⁹ without the assumption of Equation (5), dubbed the "kinetic model". Ultimately, Singer et al. showed that even across the wide span of methane phases and densities explored, the relaxation rates are quite accurately predicted by both models; implying that Equation (5) largely holds for even the lowest density system studied previously. The final SR rate equation used in this work is identical to the diffusion model equation of Singer et al. when applied to a spherical top molecule. The derivation continues as follows.

As with other mechanisms of NMR relaxation, the longitudinal rate is proportional to the spectral density (SD) of the corresponding interaction at the Larmor frequency. The SDs are formally half-

Fourier transforms of the auto-correlation functions

$$a_m = (-1)^m \int_0^\infty \langle A_m(t) A_{-m}(t+\tau) \rangle e^{im\omega\tau} d\tau \tag{7}$$

However, in the fast motion (extreme narrowing) limit they are independent of frequency and simplify to definite time integrals.

$$a_m = (-1)^m \int_0^\infty \langle A_m(t) A_{-m}(t+\tau) \rangle d\tau \tag{8}$$

The fast motion limit holds for small molecules in non-viscous liquids and high density gasses. As suggested by Mammoli et al.²¹ and shown later in our analysis of water vapor, slow decorrelation of angular momentum in dilute gasses is outside of this fast motion regime.

If rotations about different molecular axes are not correlated with one another, the SDs can be reformulated in terms of the Cartesian axes defined by the molecular moment of inertia which is also the frame in which the spin rotation tensor c_{ij} is commonly considered. Combining Equations (2) and (8) gives

$$a_0 = a_z = \sum_j c_{zj}^2 \int_0^\infty \langle J_z(t) J_z(t+\tau) \rangle d\tau$$
 (9a)

$$a_{\pm 1} = \frac{1}{2}(a_x + a_y) = \frac{1}{2} \sum_{i} c_{xj}^2 \int_0^\infty \langle J_x(t) J_x(t+\tau) \rangle d\tau + c_{yj}^2 \int_0^\infty \langle J_y(t) J_y(t+\tau) \rangle d\tau$$
 (9b)

This assumption is strongest when the principal moments of inertia are significantly different in magnitude. Also inherent here is the assumption that the spin rotation tensor is essentially constant on the order of the angular momentum correlation time, allowing it to be factored out of the time integral. If this approximation is avoided, the SR tensor remains part of the time-dependent spin operators, $A_m(t)$, and must be explicitly included in the correlation functions as in Equations (7) and (8). In the context of computing rates from MD trajectories, one could consider performing ab initio calculations of the SR tensor for molecules in all sampled MD snapshots to account for its time dependence. This was ultimately decided to be outside the scope of the current work, and the molecule-fixed SR tensor is assumed to be virtually constant for a given molecule type throughout an MD simulation.

The relaxation rates in the fast motion limit can then be formulated as

$$\frac{1}{T_1} = \frac{1}{T_2} = \frac{2}{3} \sum_{i,j=x,y,z} \sum c_{ij}^2 \int_0^\infty \langle J_j(t) J_j(t+\tau) \rangle d\tau$$
 (10)

with c_{ij} and J_i once again being Cartesian components of the spin-rotation tensor and molecular angular momentum respectively in the principal axis system of the I tensor. For gasses with lags between molecular collisions such that $\tau_c\omega_0$ is *not* much smaller than 1, the SD is frequency-dependent in the region of the Larmor frequency. Therefore, to compute the relaxation rate, the SDs must be computed explicitly via (half-) Fourier transform of the ACFs, and evaluated at the Larmor frequency (or in this case the difference of the nuclear Larmor frequency, ω_0 , and the rotational Larmor frequency, ω_J).

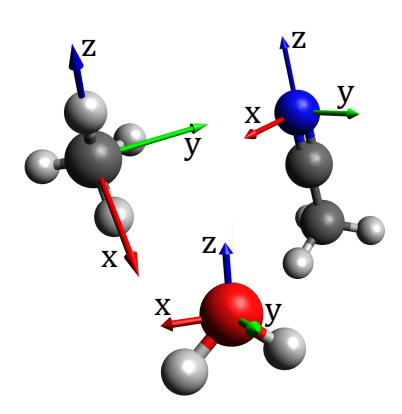


Figure 1: Molecule-fixed axis definitions used for tracking angular momentum of methane, acetonitrile, and water.

Combined with the notation introduced in Equations (9a) and (9b), Equation (10) is then written as

$$\frac{1}{T_1} = \frac{2}{3} \sum_{i,j=x,y,z} \sum_{i,j} c_{ij}^2 a_j (\omega_0 - \omega_J)$$
 (11)

with some form of the SD functions, $a_j(\omega)$. This is the theoretical formulation employed in the current work for computing SR relaxation rates of low density water vapor. If the total angular momentum correlation function is assumed to be mono-exponential, which is *not* assumed in this work, the SD can be evaluated analytically as a Lorentzian. This, along with an average magnitude of angular momentum determined by Boltzmann statistics, leads to the following rate equation utilized by Mammoli et al.²¹

$$\frac{1}{T_1} = \frac{8\pi^2 I_0 kT}{\hbar^2} C_{\text{eff}}^2 \frac{\tau_1}{1 + (\omega_0 - \omega_I)^2 \tau_1^2}$$
(12)

where a singular correlation time representing the total angular momentum and a corresponding effective SR constant are employed. Note here, $C_{\rm eff}$ is in cycles/s, while elsewhere, components of the SR tensor are in radians/s. See Supporting information (SI) for an example definition of $C_{\rm eff}$.

In this work, the Cartesian components of the molecular angular velocities are obtained from an atomistic MD trajectory following Singer et al., 12 via solution of the matrix equation

$$\sum_{Q} \begin{pmatrix} y_Q^2 + z_Q^2 & x_Q y_Q & x_Q z_Q \\ y_Q x_Q & x_Q^2 + z_Q^2 & y_Q z_Q \\ z_Q x_Q & z_Q y_Q & x_Q^2 + y_Q^2 \end{pmatrix} \begin{pmatrix} \omega_x \\ \omega_y \\ \omega_z \end{pmatrix} = \begin{pmatrix} \sum_{Q} (\mathbf{r}_Q \times \mathbf{v}_Q)_x \\ \sum_{Q} (\mathbf{r}_Q \times \mathbf{v}_Q)_y \\ \sum_{Q} (\mathbf{r}_Q \times \mathbf{v}_Q)_z \end{pmatrix}$$
(13)

where the sums are over all atoms, Q, in a given molecule, and x_Q , y_Q , z_Q are positions relative to the molecular center of mass (CoM). This equation is solved for each molecule at each sampled frame of the dynamics to obtain the angular velocity components, ω_k . Furthermore, \mathbf{r}_Q and \mathbf{v}_Q are atomic position and linear velocity vectors, respectively, relative to the molecular CoM.

For the purpose of consistently tracking the correlation of rotation about chosen molecular axes,

the formalism may be equivalently represented in a molecule-fixed coordinate system for which the ordering of the principal axes is tied to unique atoms and remains constant for each molecule throughout the trajectory. The coordinate systems chosen are defined as shown in Figure 1. Since the SR tensor and angular momentum must share the same principal axis system, the SR tensor, C, must also be rotated from the moment of inertia frame in which it is calculated to the selected molecule-fixed frame. We took the described approach in our implementation and it is summarized as follows.

First, the SR tensor for a given molecule, in the moment of inertia frame, C_I , as computed with Dalton⁴⁴ (see Section 3) must be redefined in the lab frame via a transformation matrix, T, made up of column eigenvectors of the moment of inertia tensor, I.

$$C_{lab} = T C_I T^{-1} \tag{14}$$

The molecular moment of inertia tensor is defined as

$$I = \begin{pmatrix} I_{xx} & I_{xy} & I_{xz} \\ I_{yx} & I_{yy} & I_{yz} \\ I_{zx} & I_{zy} & I_{zz} \end{pmatrix} = \sum_{Q} \begin{pmatrix} m_{Q}(y_{Q}^{2} + z_{Q}^{2}) & m_{Q}(x_{Q}y_{Q}) & m_{Q}(x_{Q}z_{Q}) \\ m_{Q}(y_{Q}x_{Q}) & m_{Q}(x_{Q}^{2} + z_{Q}^{2}) & m_{Q}(y_{Q}z_{Q}) \\ m_{Q}(z_{Q}x_{Q}) & m_{Q}(z_{Q}y_{Q}) & m_{Q}(x_{Q}^{2} + y_{Q}^{2}) \end{pmatrix}$$
(15)

where m_Q are atomic masses. Then, a rotation operator, R, is defined which transforms the chosen molecule-fixed frame, M, into the moment of inertia frame,

$$MR = T \tag{16}$$

And finally, the inverse rotation matrix is applied to the Cartesian SR tensor to obtain the SR tensor in the molecule-fixed frame:

$$C_{\text{mol}} = R C_{\text{lab}} R^{-1} \tag{17}$$

In the ab initio calculations, an individual SR tensor is obtained for each proton in the molecule. The relaxation rate calculations are carried out with either Equation (10) or (11) using the transformed SR tensor at each proton and averaged to obtain the total relaxation rate.

3 Methods

Car Parinello aiMD (CPMD) simulations of water and acetonitrile used in this work are the same as those developed and sampled in our previous work.⁴ They were performed using the Quantum Espresso⁴⁵ (QE) package (Version 6.0). Water simulations contained 64 molecules in a cubic cell, and acetonitrile simulations contained 32 molecules. Ten independent trajectories for each system were run starting with 5 ps of equilibration in NVT at 300K followed by 1 ps further equilibration in NVE. Simulations were continued in NVE, to give production run times of 20 ps for water simulations and 16 ps for acetonitrile. For full computational details on QE simulations, see Ref. 4. Additional aiMD simulations of the Born-Oppenheimer (BO) type using the CP2K⁴⁶ package (Version 8.2) have since

been developed for water and acetonitrile; taking advantage of better performance and longer simulation time steps in order to explore longer simulation times and various exchange-correlation (XC) functionals. CP2K simulations use a mixed atom-centered (DZVP) and plane-wave basis. All aiMD simulations contain 64 molecules (doubling that of the QE acetonitrile simulation, resulting in a corresponding cell dimension of 17.71Å). The time step was 1 fs in the acetonitrile simulations and 0.5 fs in the water simulations. Dispersion corrections were included using Grimme's D3 correction.⁴⁷ Protocol for setup and equilibration of the MD trajectories followed those established in previous work, including random packing, partial optimization, and pre-equilibration with force-field (FF) MD in Tinker.⁴⁸ The BOMD was initialized with 50 steps of Langevin dynamics at 300K (temperature tolerance of \pm 10K). This was followed by 5 ps of simulation in the NVT ensemble at 300K using the canonical sampling through velocity rescaling (CSVR) thermostat⁴⁹ with a time constant of 10 fs. Finally, the production phase was simulated in the NVE ensemble in which the first 1 ps was taken to be further equilibration time. Total production times for BOMD water simulations across independent trajectories and investigated XC functionals are in the range of 15-20 ps. Production times for acetonitrile are 20 ps. Simulations of methane in variable phases and pressures as well as gas-phase water simulations were run entirely with FFMD in Tinker. Simulations contained 200 molecules each and cell dimensions were chosen such that pressures equaled the target experimental pressure assuming ideal behavior. Average pressures calculated on the fly in Tinker were consistent with these target pressures within a few kPa (see SI). Sampled production times were in the NVE ensemble and totaled between 20-50 ps across the methane simulations. Water vapor simulations had production runs of 20 ns. Single-point KS DFT calculations were performed with Dalton⁴⁴ to determine SR tensors for gas phase optimized structures for methane, acetonitrile, and water. The 3 parameter hybrid XC functional of Becke, Lee, Yang, and Parr (B3LYP)⁵⁰ and the IGLO III basis set⁵¹ were employed for these calculations.

4 Results and Discussion

Figure 2 summarizes the relaxation results for the sampled methane systems (classical MD), broken down by dipolar and SR mechanisms, and compared to the total measured rates. The overall agreement with experiments is good, with the largest overestimations for the coldest liquid phase system and lowest-pressure gas system. The greatest underestimation is for the lower pressure supercritical (SC) system. To our knowledge, an experimental breakdown of the contributing mechanisms, at least for these specific temperatures and pressures, is not available in the literature, therefore a quantitative comparison of the mechanistic breakdown is not possible at present. However, the theory clearly allows for qualitative and quantitative analysis. In the low-temperature liquid, the dipolar contribution dominates, in particular the intermolecular portion, because of retarded rotational motion and longer, more frequent contacts between protons on neighboring molecules. In the middle range of temperature and pressure (i.e. liquid at 143K and high pressure SC phase), dipolar and SR contributions are roughly equal. In the two lowest pressure systems, the SR mechanism dominates because of relatively large average distances between molecules and fast molecular rotation modulated by comparatively infrequent molecular collisions.

Figure 3a shows the computed angular momentum correlation functions which determine the SR contribution to the methane relaxation. The relatively small error bars here and in all following plots of correlation functions are determined by the standard error in the mean across ten independent simulations. Therefore, it should be noted that this procedure only serves to estimate the statitistical error in the sampling of the dynamics and not systematic errors inherent in the computational methods or approximations in the theory. Figure 3b shows the corresponding SDs given by half-Fourier transform of the ACFs, and plotted on a log scale on the frequency axis. In all but the gas-phase simulation, the available sampling allows for a clear resolution of the full dispersion region of the SD, and at least some extension into the low, frequency-independent region. In any case, since typical proton Larmor frequenies are on the order of 10^2 MHz or 10^{-4} ps⁻¹, relaxation in all of these simulated methane systems is well described within the extreme narrowing limit. Therefore the SR rates are proportional to the correlation times as determined from these correlation functions. The correlation times represent the average time between molecular collisions that transfer angular momentum between colliding partners. The correlation functions for methane can reasonably be approximated as mono-exponential, as confirmed by the linear fits in the semi-log plot of Figure 4. Angular momentum correlation functions and SDs are plotted for aiMD liquid acetonitrile and water in Figures 5 and 6 respectively. Here, nonshperical molecular symmetries require separation of the angular momentum components according to the molecule-fixed coordinates defined in Figure 1. Both systems have more complex oscillatory features in their correlation functions which are also reflected as peaks in the high-frequency region of the SDs. In acetonitrile, the angular momentum ACF associated with rotation of the C–C–N (z)axis exhibits a sub-picosecond oscillation, indicating some hindered transfer of angular momentum at this time scale. The relative noisiness of the orthogonal axes and resultant sharp peaks in the SD are caused by C-H vibrations and the method used to define the dynamic molecular axis system from

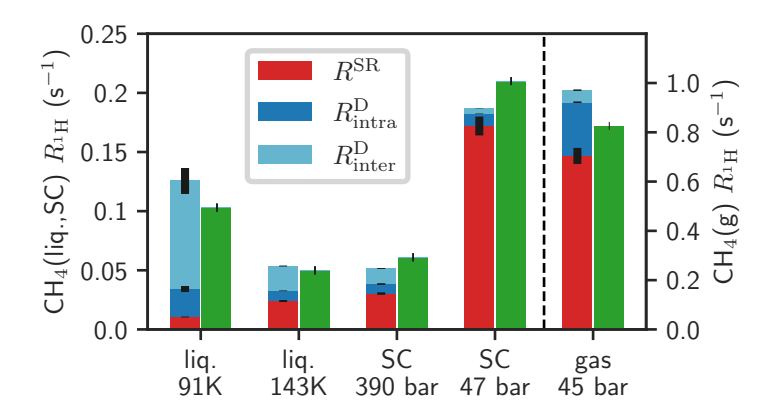


Figure 2: Summary of calculated (left bar in each pair) and experimental (right green bars) R_1 for ¹H in methane. Calculations are from sets of classical simulations. Theoretical results are broken down by contributing mechanism (SR, intramolecular dipolar, and intermolecular dipolar). Values for gaseous methane are plotted on a separate axis (right). Experimental values are from Ref. 12

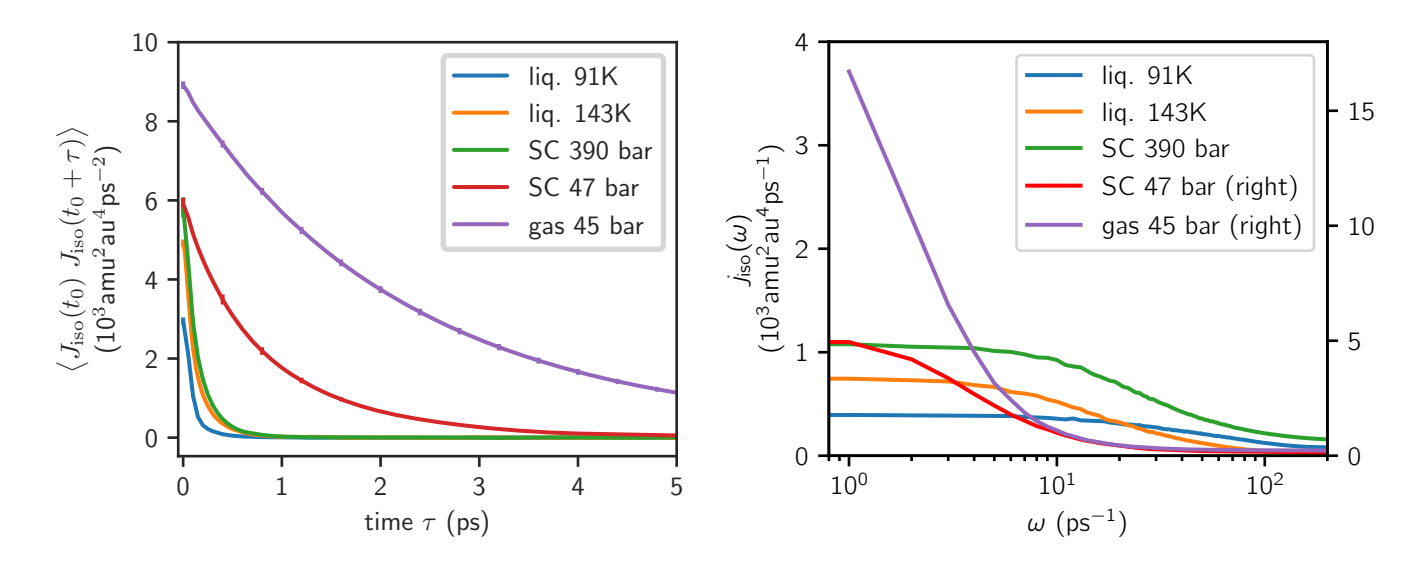


Figure 3: Average isotropic angular momentum correlation functions (left) and corresponding spectral densities (right) for methane for sets of classical simulations corresponding to Figure 2.

the bond vectors. The ACF components for liquid water have unique oscillatory features which agree qualitatively with angular velocity ACFs reported in the literature.⁵²

The overall relaxation results for acetonitrile and water, determined at different levels of theory and with two different QM codes, are provided in Figure 7. Once again, the results are broken down by mechanism and compared to experimental values for which the mechanistic breakdowns are available in this case. For acetonitrile, the computed SR contribution obtained from MD in QE and in CP2K are nearly equivalent, while a somewhat greater dipolar contribution is obtained with CP2K and the revPBE functional. The computed SR contribution is larger than the experimentally determined estimate by about a factor of 2 in both sets of calculations, while the dipolar contributions are more closely

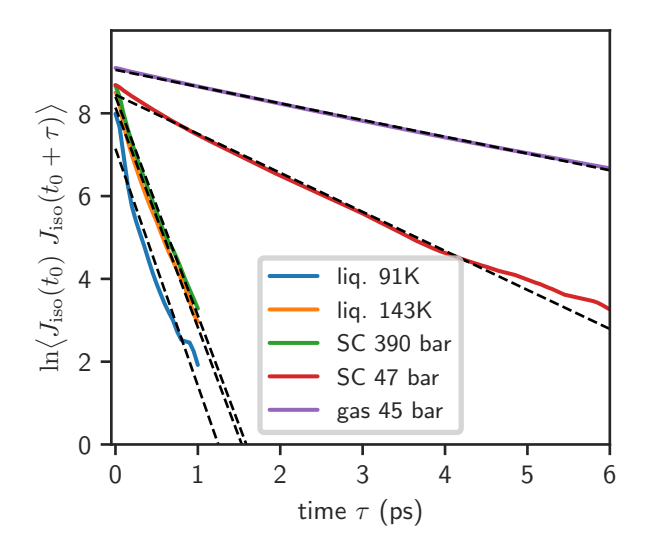


Figure 4: Semi-log plot of methane correlation functions from Figure 3. Linear least-squares fits are plotted and have the following numerical slopes in the chosen axis units: Liq. 91K: -5.73; liq. 143K: -5.31; SC 390 bar: -5.29; SC 47 bar: -0.94; gas 45 bar: -0.40

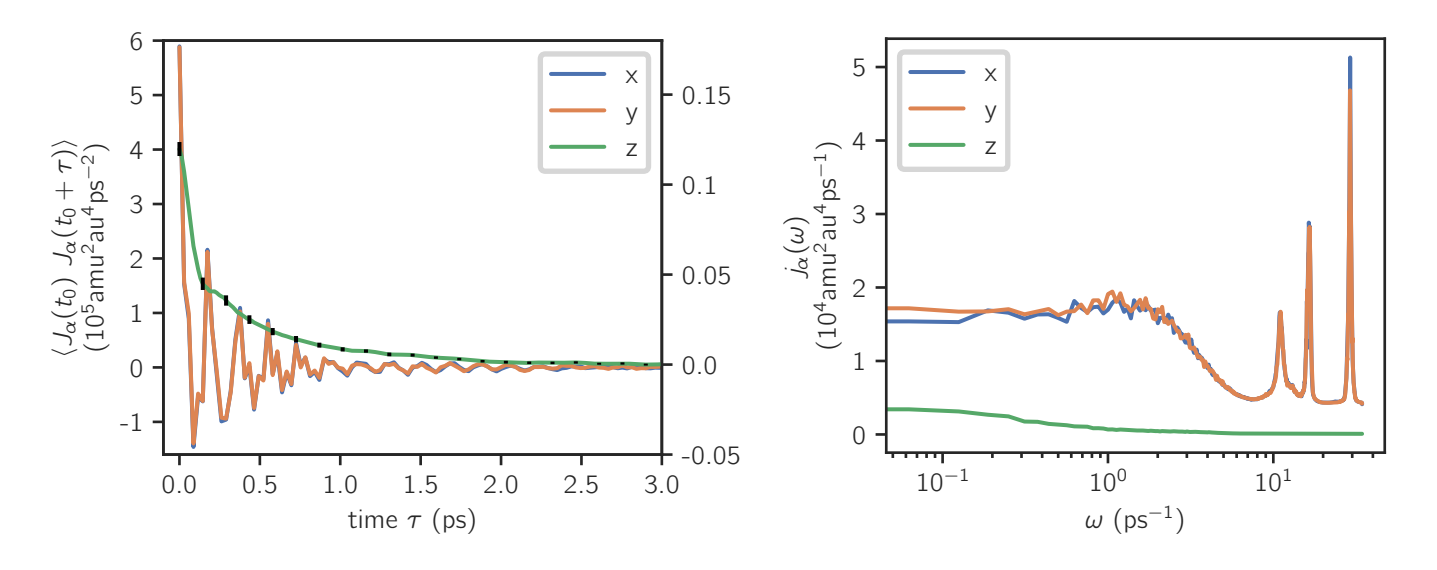


Figure 5: Angular momentum correlation functions (left) and corresponding spectral densities (right) for acetonitrile molecules in sets of liquid phase CPMD simulations at 300K. Total angular momentum is broken down to components corresponding to the molecular axis system defined in Figure 1. The z component correlation function is plotted on a different scale (right).

predicted by CP2K/revPBE. However, the total calculated relaxation rates agree well with the experimental value, which raises the question whether the experimental breakdown into SR and dipolar contributions is worth re-examining. The SR contribution is known to be negligible in liquid water, and this is reflected in our calculations. Again, CP2K/revPBE gives the closest agreement with the experimental dipolar contributions.

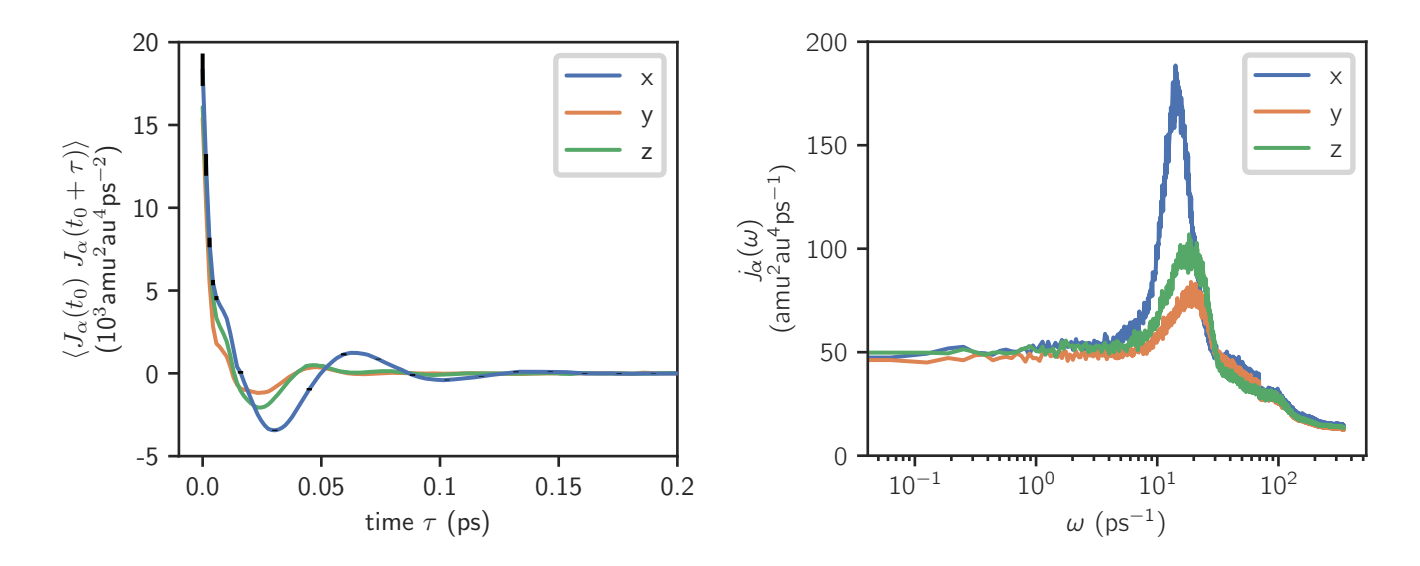


Figure 6: Angular momentum correlation functions (left) and corresponding spectral densities (right) for water molecules in sets of liquid phase CPMD simulations at 300K. Total angular momentum is broken down to components corresponding to the molecular axis system defined in Figure 1.

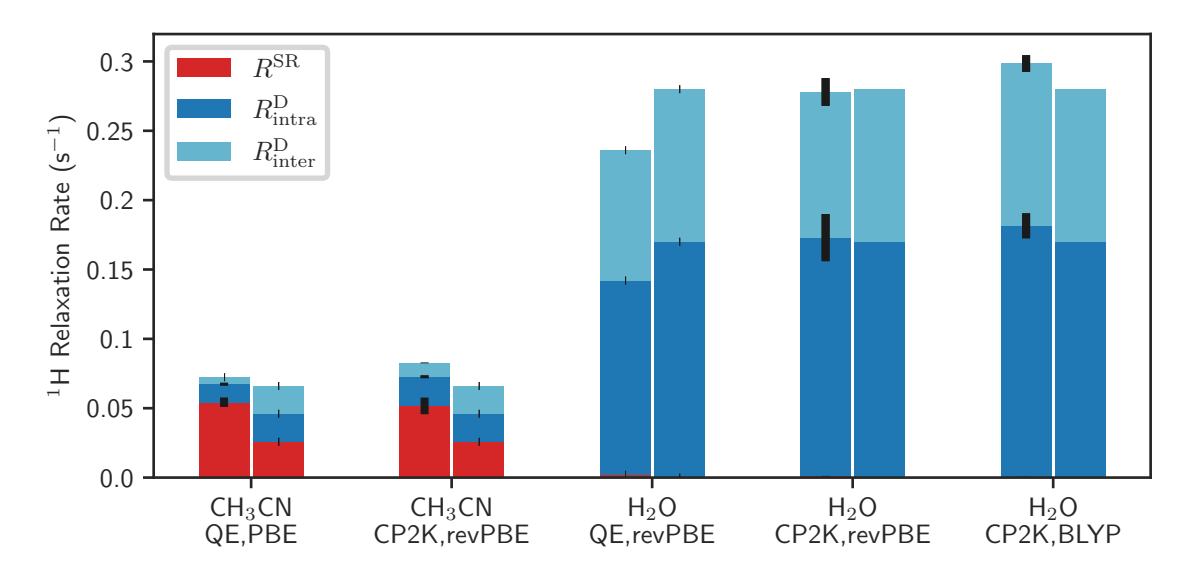


Figure 7: Summary of calculated (left bar in each pair) and experimental (right bars) R_1 for 1 H in acetonitrile and water at various levels of theory in aiMD. Results are broken down by contributing mechanism (SR, intramolecular dipolar, and intermolecular dipolar. Experimental results are from Ref. 15

Perhaps the most interesting result of this work is from our calculation of SR relaxation in water vapor systems, for which the SR mechanism is dominant, and whose experimental values (of T_1) were measured apparently for the first time relatively recently by Mammoli et al. As discussed in Section 2, low-density systems have slow decorrelation of molecular angular momentum due to relatively rare molecular collisions. Therefore the extreme narrowing condition does not necessarily hold and the

at the Larmor frequency is not equal to that at zero frequency, the SDs must be computed explicitly as half-Fourier transforms of the ACFs. Longitudinal relaxation is then computed by the value of the SD at the relevant Larmor frequency, which in this case is the difference between the nuclear Larmor frequency, ω_0 , and the molecular rotational Larmor frequency, i.e. $\omega_0 - \omega_J = 7 \times 10^{-4} \text{ ps}^{-1}$, as reported in Ref. 21 for the corresponding experimental measurements. In order to obtain sufficient sampling of the SD at this low frequency, long simulation times (here 20 ns) are required. Figure 8 shows the calculated ACFs for the 2 kPa simulation as well as the corresponding SDs, plotted as discrete points in order to indicate the limited sampling in the low-frequency region. A vertical dashed line is added at the value of the experimental Larmor frequency at which the value of the SD is sampled for use in Equations (11) and (18). The time scale on which the ACFs are plotted (and therefore the correlation times) is four orders of magnitude greater than for any of the liquid systems. On this scale, the *z*-component, representing the principal rotation axis and intermediate moment of inertia axis of the water molecule, decays nearly instantly. The remaining two components decay over a few nanoseconds.

Applying Equation (11) for classical gaseous water simulations at various temperatures and pressures yields the results plotted in Figure 10. Experimental values are those of Ref. 21 and the fitted curves are of the form of Equation (12) combined with the relationship $\tau_1 = p^{\text{max}}/[p (\omega_0 - \omega_J)]$ as defined in Ref 21, where p^{max} is a fit parameter corresponding to the pressure which results in the maximum value of R_1 . The agreement with experiment is remarkable, despite the calculations containing no explicit consideration of the orientational correlation functions. Our calculations also confirm relaxation in the gas phase is completely dominated by the SR mechanism, with calculated dipolar contributions at 47 kPa for example, totaling only about $0.6 \, \text{s}^{-1}$. An additional simulation with a pressure of 2 kPa (well below p^{max}) was considered and found to lie reasonably well on the curve from theory, which was fitted excluding this low-pressure data point for which there is no available experimental result. This our predicted magnitude of the longitudinal relaxation rate at 2 kPa. It should be noted that in both these calculated results and the Mammoli et al. measurements, no statistically significant temperature dependence is observed for the relaxation rate in water vapor at the densities and the temperature range considered.

We predict from the same data set the transverse relaxation rate R_2 for the water vapor systems. R_2 is calculated as a sum of terms proportional to the SD at the Larmor frequency, and the SD at zero frequency respectively.^{53,54} The expression is as follows:

$$R_2 = \frac{1}{T_2} = \frac{1}{3} \sum_{i,j=x,y,z} \sum c_{ij}^2 j_j(\omega_0 - \omega_J) + \frac{1}{3} \sum_{i,j=x,y,z} \sum c_{ij}^2 j_j(0)$$
 (18)

In the simplified formalism analogous to Ref. 21 and Equation (12), the previous result can be written as

$$R_2 = \frac{1}{T_2} = \frac{4\pi^2 I_0 kT}{\hbar^2} C_{\text{eff}}^2 \left[\frac{\tau_1}{1 + (\omega_0 - \omega_J)^2 \tau_1^2} + \tau_1 \right]$$
 (19)

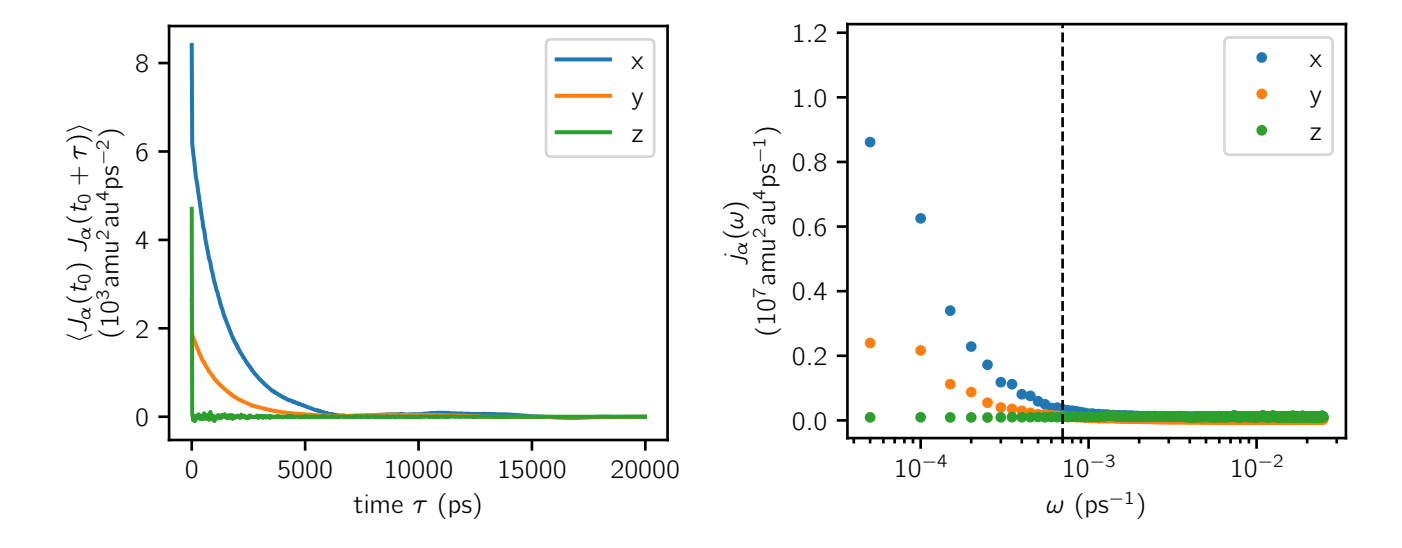


Figure 8: Angular momentum correlation functions (left) and corresponding spectral densities (right) for water molecules in FFMD water vapor simulations at 2 kPa. The gas-phase SD is plotted as discrete points to indicate the lack of sampling in the low-frequency region, resulting from the finite time scale of the simulation. The dotted vertical line indicates the experimental Larmor frequency reported in Ref. 21 and used in our relaxation rate calculations.

The results are plotted in green along with the calculated R_1 results in Figure 11. As expected from simple relaxation theory, R_1 and R_2 converge on the right side of p^{\max} , as the fast motion limit is approached. On the left of p^{\max} , R_2 continues to increase with decreasing pressure while R_1 sharply decreases.

As mentioned in Section 2, SR relaxation in gas phase systems with angular momentum autocorrelation in the slow-motion regime are expected to have an important contribution from reorientational correlation functions. However, these were not considered for the calculated results in Figures 10 and 11. Indeed, we confirm that the coupled correlation function contained in Equation (4) can not be decoupled according to Equation (5), in the case of gas phase simulations, while the approximation does hold as expected for the liquid. This result is summarized in Figure 9 in which the decoupled product of angular momentum and orientational correlation functions is plotted alongside the corresponding cross-correlation function for both the aiMD liquid (left) and classical gas phase simulations (right). Here, the quantity J is shorthand for the J_{-1} component of the angular momentum in the irreducible representation. D is shorthand for of the $\mathcal{D}_{0,1}$ component of the rank 1 Wigner \mathcal{D} matrix; the autocorrelation of which is effectively the first-order rotational ACF. It is clear from these plots that the condition of Equation (5) holds within statistical error in our liquid simulations, while a significant deviation in the two curves is observed in the gas phase.

The accurate results in Figure 10 with respect to experiment are attributed to the fact that the molecular SR tensor for water is nearly isotropic, i.e. $c_{xx} \approx c_{yy} \approx c_{zz}$ in the molecule-fixed reference frame. As discussed in Section 2 and shown in the literature by Hubbard²⁷ and others, when the SR tensor has a weak orientational dependence, only the angular momentum correlation functions con-

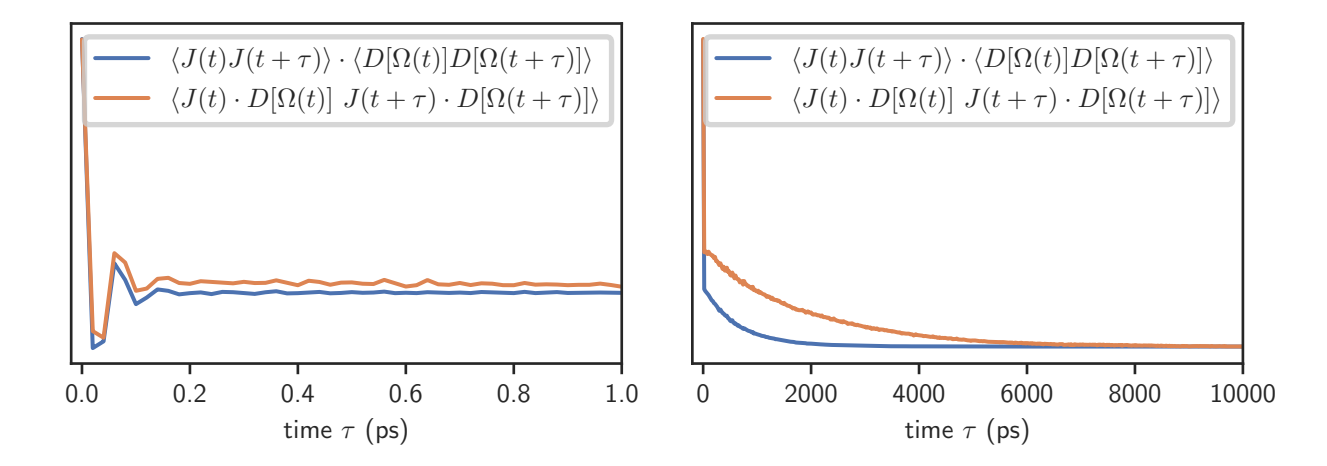


Figure 9: Calculated product and cross-correlation functions between molecular angular momentum and orientation for simulated liquid water (left) and water vapor (2 kPa) (right). Correlation functions are computed for the J_{-1} component in the irreducible representation of the angular momentum components and the $\mathcal{D}_{0,1}$ component of the rank 1 Wigner \mathcal{D} matrix.

tribute to the relaxation mechanism. Therefore, our results for gas-phase water are in good agreement with the experiments not by accident, but because the reorientational correlation functions hardly contribute to the relaxation rate for a system with a nearly isotropic SR tensor. The same analysis was performed for simulations of low-density methane, for which the SR tensor is highly anisotropic, despite the higher geometric symmetry of the tetrahedral molecule. Resulting rates in the region of the characteristic maximum and below were significantly underestimated. These results are provided in the SI.

Mammoli et al. used their relaxation results for predictions of the collisional cross-section, σ_I , of molecules in water vapor. Such collisions drive the SR relaxation process and therefore we found it appropriate to investigate the nature of these collisions in our MD. An analysis was performed to probe collisions in the first nanosecond of the 353K, 47 kPa water vapor simulation. First, the angular momentum time series data were analyzed to identify, for each molecule, times at which a significant change of root-mean-square angular momentum occurs about any one of the molecule-fixed axes. A value of 10 rad amu bohr²/ps = 0.89 amu $Å^2$ /ps was chosen to be the threshold for a 'reactive' collision, i.e., a collision that contributes to the SR relaxation mechanism by changing the angular momentum and thus contributing to the decorrelation. The chosen value is roughly 10% of the maximum jump of angular momentum found within the trajectory. Next, time windows defined as 5 ps before and after each identified event were searched, and the closest intermolecular distance in the time window tallied. The results are plotted as a histogram in Figure 12, with stacked colored bars corresponding to the type of atom-to-atom contact found to be closest. Intermolecular distances up to a cutoff of 50Å were searched. Somewhat surprisingly, a long tail is seen in the histogram out to distances reaching this cutoff distance (see inset of Figure 12). As a result, the mean distance for the full population of counted events is 12.6Å, while the median is 6.8Å, and the most probable interaction distance for

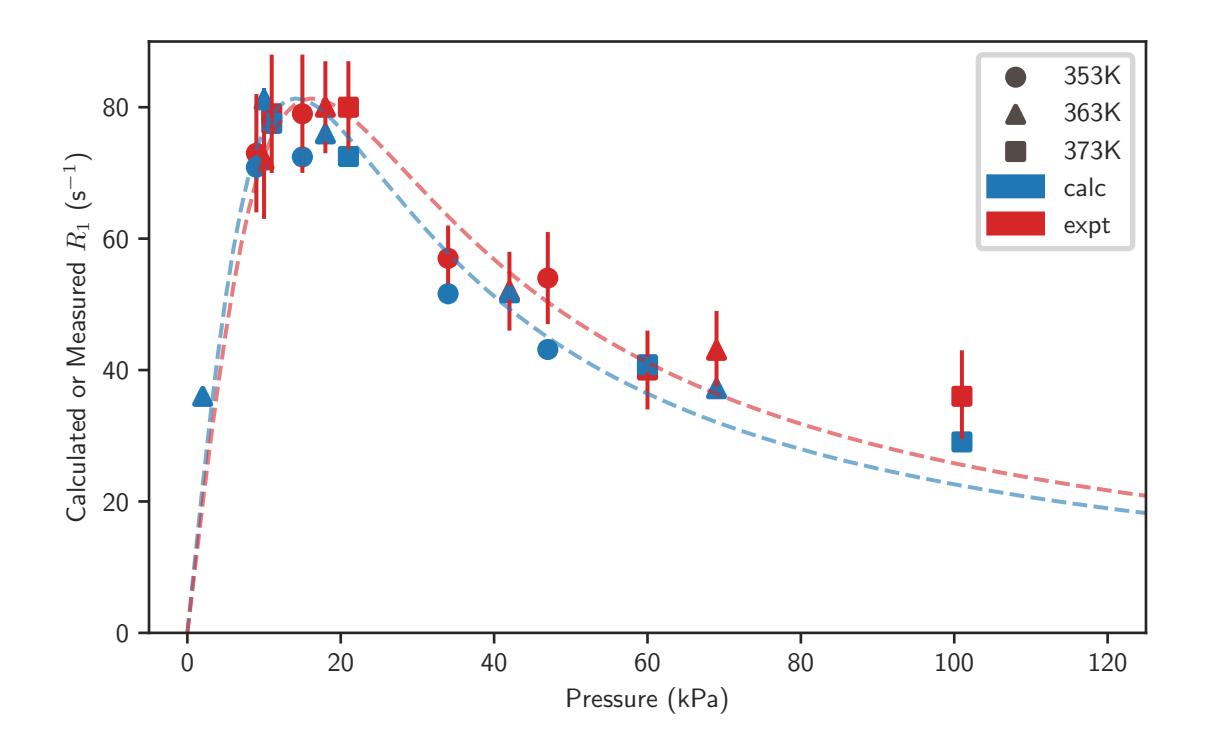


Figure 10: Calculated and experimental R_1 of ¹H in water vapor versus pressure and at three different temperatures. Calculations are from sets of 20 ns classical simulations. The dashed curve is a fit based on Equation (12) with the substitution $\tau_1 = p^{\text{max}}/[p(\omega_0 - \omega_J)]$. Experimental values are from Ref. 21

events of angular momentum transfer is also the closest at about 2Å. Another peak occurs in a broader range over 4–8Å. There is a trough between 3–4Å implying that two-body interactions which transfer angular momentum will likely fall into one of the two peak regions on either side when only the single closest distance of approach is considered. In the region below 3Å, the mean distance is 2.1Å for both O-H and H-H contacts and the ratio of O-H to H-H frequency is 1.13. In the region above 4Å, the mean distance is 11.3Å for O-H contacts and 17.6Å for H-H contacts. The ratio of O-H to H-H frequency in this region is about nine times smaller at 0.12. Two-body events that occur farther than 4Å are dominated by Van der Waals interactions, and should not be considered steric collisions. At these distances, it is sensible that an H-H distance is the shortest in the course of two mutually rotating water molecules passing one another and interacting weakly. Events captured in the tail region of Figure 12 are extremely long-distance as to unlikely be two-body events at all. A possibility that requires further study is that, in a uni-molecular process, angular momentum may be transferred to vibrational energy via rovibrational modes. This type of transfer would in principle contribute to the SR relaxation. Events that occur shorter than 3Å are driven by Coulomb and overlap interactions, for which O-H contacts are expected to dominate. O-O contacts as the shortest intermolecular distance during an angular momentum transfer is apparently exceedingly rare.

If the overall average intermolecular distance is considered as the mean interaction radius, a σ_J of 503Å² is obtained for interactions which contribute to SR relaxation. To supplement this result, σ_J

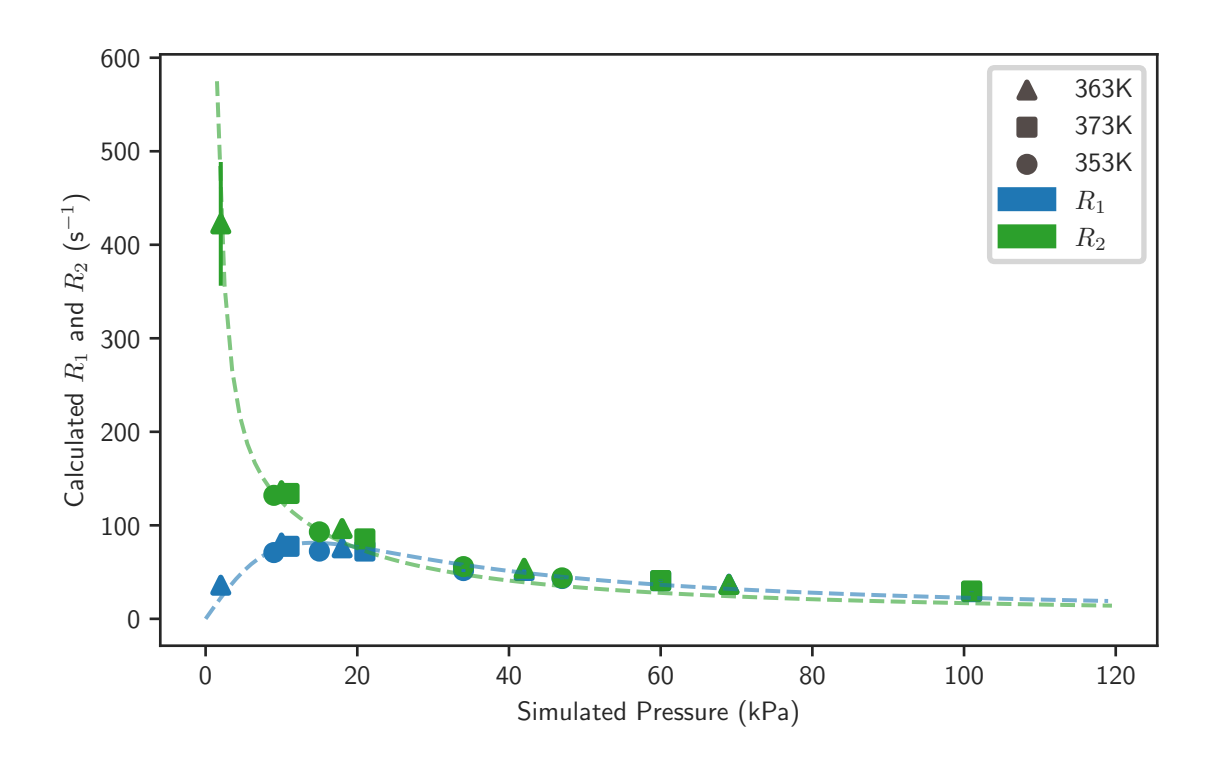


Figure 11: ¹H R_1 and R_2 calculated from sets of 20 ns classical water vapor simulations at various pressures. The dashed curve for R_1 and R_2 are fits based on Equations (12) and (19) respectively with the substitution $\tau_1 = p^{\text{max}}/[p(\omega_0 - \omega_J)]$. Experimental values are from Ref. 21

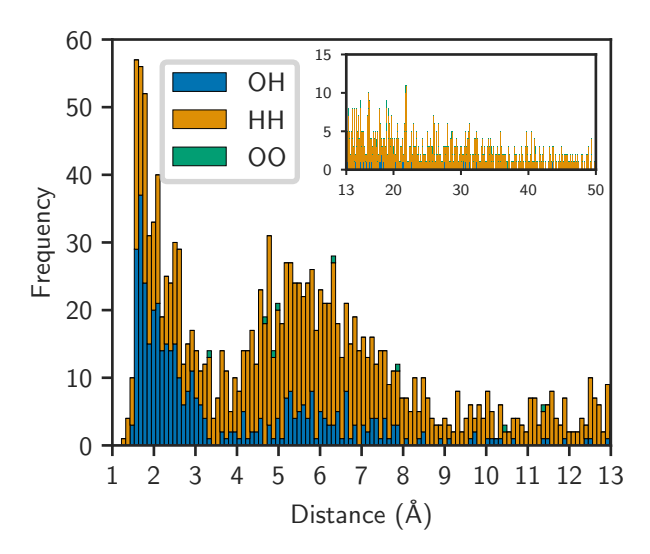


Figure 12: Histogram counting the number of two-body events in water vapor simulation (47kPa,353K) which result in a change in molecular angular momentum and the shortest atom-to-atom distance during the event. Events are categorized by the particular atom pair which defines the shortest distance in a 20 ps window around the sampled event. The inset shows the long-distance tail of the data out to the numerical cutoff of 50Å

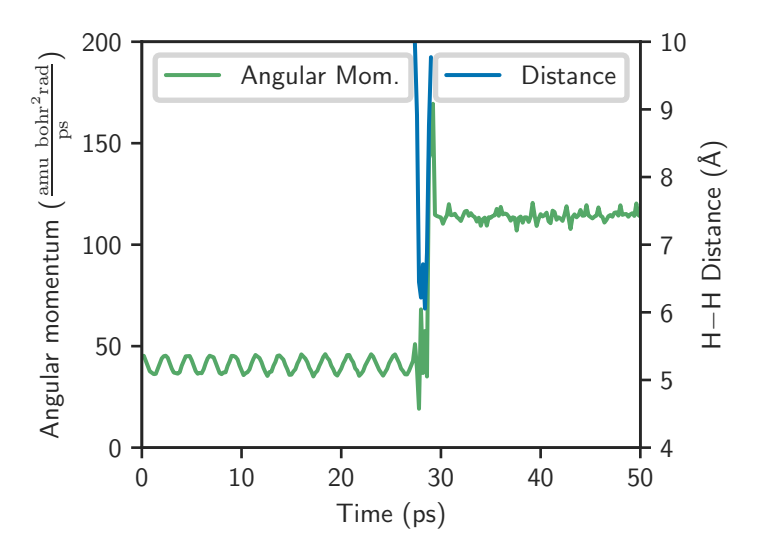


Figure 13: Magnitude of angular momentum, *J*, of a particular molecule in a water vapor simulation plotted with the H–H distance to another molecule at the point of a collision event around 25-30 ps during which angular momentum is transferred.

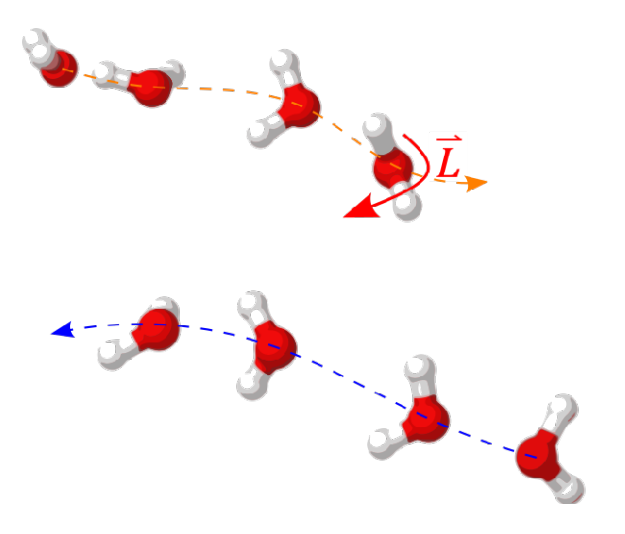


Figure 14: Sketch of the event in water vapor described by Figure 13 in which the top molecule experiences a discontinuous change in angular momentum due to proximity of another molecule.

was computed from the dynamics in the traditional way following the formula

$$\sigma_J = \frac{1}{\rho \,\bar{\nu} \,\tau_J} \tag{20}$$

Here, ρ and $\bar{\nu}$ are the number density and mean thermal velocity of the system respectively, and τ_J is the correlation time associated with changes in molecular angular momentum. For the system in question, integration of the vector ACF of the angular momentum gives $\tau_J = 34.7$ ps. Equation (20) then gives $\sigma_J = 435\text{Å}^2$, corresponding to an average interaction radius of 11.8Å. The cross-section re-

sults obtained from both methods described above are 3–4 times larger than the estimate in Reference 21. Mammoli et al. possibly underestimated σ_J due to a simplified relaxation model based on equation 12 which assumes a mono-exponential ACF, resulting in a reported τ_J of 82 ps; over two times our simulated result.

Figure 13 shows the magnitude of angular momentum, J, of a representative water molecule in a segment of the water vapor simulation. Additionally, the distance from a hydrogen in the analyte molecule to a hydrogen of a colliding neighbor is plotted. A clear jump in the angular momentum can be seen during the close-contact period. The distance of this contact is decidedly larger than typical steric interactions and consistent with the second region of interaction events seen in Figure 12. When this 'collision' in the dynamics is isolated and visualized, it is seen that the transfer of angular momentum occurs as two water molecules pass each other at this distance of roughly 6 Å. Figure 14 is a representation of this particular event taken from the MD trajectory. As the two molecules pass, the one depicted above spins up and leaves the interaction with markedly faster rotational motion. Whether or not these kinds of interactions are physical or artifacts from the parameterized force field used in the MD is not easy to prove. However, the strong agreement achieved with the experimental relaxation rates suggests that, on the whole, the interactions driving the SR mechanism are well modeled in the MD.

5 Summary, Conclusions, and Outlook

A robust method for computing SR NMR relaxation rates from molecular dynamics simulations was developed and applied to ¹H NMR relaxation in canonical molecular systems in a wide range of temperatures and pressures. Combined with similar methods for the dipolar mechanism, a unified set of results were obtained for water, methane, and acetonitrile in the liquid and dense gas phases which accurately reproduce the experimental results. Low density water vapor systems were also investigated and while the angular momentum autocorrelation was found to be in the slow-motion regime, accurate results with respect to experiments by Mammoli et al. were obtained without consideration of orientational correlation functions. It is expected that gas phase systems such as methane or acetonitrile at equivalent pressures would indeed require a contribution from molecular reorientation due to the fact that their SR tensors are anisotropic. Based on our results, the collisional cross-section relevant for the interactions driving SR relaxation in water vapor at 353K was predicted to be larger than previous experimental estimates. We plan to continue to augment our methods with more generalized theory. Future work will include implementation of a fully generalized SR theory which considers the coupled molecular angular momentum and orientational correlation functions.

Acknowledgments

The authors acknowledge the Center for Computational Research (CCR) at the University at Buffalo for providing computational resources, in particular those made available via grant MRI-1724891 from

the National Science Foundation (NSF). This work has been supported by NSF grants CHE-1855470 and CHE-2152633.

Supporting Information

Optimized XYZ format structures used for Dalton calculation of SR tensors. Example definition of $C_{\rm eff}$ in Equation (12). Instantaneous pressures calculated by Tinker for water vapor simulations. Trajectory data for example two-body collisions in water vapor simulations and corresponding molecular angular momentum time series plot. Relaxation results for low-density methane simulations.

References

- [1] Badu, S.; Truflandier, L. A.; Autschbach, J. "Quadrupolar NMR Spin Relaxation Calculated Using Ab-initio Molecular Dynamics: Group 1 and Group 17 Ions in Aqueous Solution". *J. Chem. Theory Comput.* **2013**, *9*, 4074–4086.
- [2] Philips, A.; Marchenko, A.; Truflandier, L. A.; Autschbach, J. "Quadrupolar NMR relaxation from ab-initio molecular dynamics: Improved sampling and cluster models vs. periodic calculations". *J. Chem. Theory Comput.* **2017**, *13*, 4397–4409.
- [3] Philips, A.; Marchenko, A.; Ducati, L. C.; Autschbach, J. "Quadrupolar ¹⁴N NMR Relaxation from Force-Field and Ab-Initio Molecular Dynamics in Different Solvents". *J. Chem. Theory Comput.* **2019**, *15*, 509–519.
- [4] Philips, A.; Autschbach, J. "Proton NMR Relaxation from Molecular Dynamics: Intramolecular and Intermolecular Contributions in Water and Acetonitrile". *Phys. Chem. Chem. Phys.* **2019**, *21*, 26621–26629.
- [5] Philips, A.; Autschbach, J. "Quadrupolar NMR relaxation of aqueous ¹²⁷I⁻, ¹³¹Xe, and ¹³³Cs⁺: A first-principles approach from dynamics to properties". *J. Chem. Theory Comput.* **2020**, *16*, 5835–5844.
- [6] Abella, L.; Philips, A.; Autschbach, J. "The sodium anion is strongly perturbed in the condensed phase even though it appears like a free ion in NMR experiments". *J. Phys. Chem. Lett.* **2020**, *11*, 843–850.
- [7] Abella, L.; Philips, A.; Autschbach, J. "Ab Initio Molecular Dynamics Study of Sodium NMR Chemical Shifts in the Methylamine Solution of [Na⁺[2.2.2]cryptand Na⁻]". *Phys. Chem. Chem. Phys.* **2021**, *23*, 339 –346.
- [8] Lo, S.-W.; Hirasaki, G. J.; House, W. V.; Kobayashi, R. "Mixing Rules and Correlations of NMR Relaxation Time With Viscosity, Diffusivity, and Gas/Oil Ratio of Methane/Hydrocarbon Mixtures". *SPE J.* **2002**, *7*, 24–34.

- [9] Hirasaki, G. J.; Lo, S.-W.; Zhang, Y. "NMR properties of petroleum reservoir fluids". *Mag. Res. Imag.* **2003**, *21*, 269–277.
- [10] Yang, Z.; Hirasaki, G. J.; Appel, M.; Reed, D. A. "Viscosity Evaluation for NMR Well Logging of Live Heavy Oils". *Petrophysics* **2012**, *53*, 22–37.
- [11] Singer, P. M.; Asthagiri, D.; Chapman, W. G.; Hirasaki, G. J. "Molecular dynamics simulations of NMR relaxation and diffusion of bulk hydrocarbons and water". *J. Mag. Res.* **2017**, *277*, 15–24.
- [12] Singer, P. M.; Asthagiri, D.; Chapman, W. G.; Hirasaki, G. J. "NMR spin-rotation relaxation and diffusion of methane". *J. Chem. Phys.* **2018**, *148*, 204504.
- [13] Singer, P. M.; Asthagiri, D.; Chen, Z.; Valiya Parambathu, A.; Hirasaki, G. J.; Chapman, W. G. "Role of internal motions and molecular geometry on the NMR relaxation of hydrocarbons". *J. Chem. Phys.* **2018b**, *148*, 164507.
- [14] Asthagiri, D.; Chapman, W. G.; Hirasaki, G. J.; Singer, P. M. "NMR 1H–1H Dipole Relaxation in Fluids: Relaxation of Individual 1H–1H Pairs versus Relaxation of Molecular Modes". *J. Phys. Chem. B* **2020**, *124*, 10802–10810.
- [15] Woessner, D.; Snowden Jr., B.; Thomas Strom, E. "A Study of Molecular Re-orientation in Liquid Acetonitrile by Nuclear Spin-lattice Relaxation". *Mol. Phys.* **1968**, *14*, 265–273.
- [16] Tiffon, B.; Ancian, B. "14N nuclear magnetic resonance study of the rotation of acetonitrile in n-alkanes". *J. Chem. Phys.* **1982**, *76*, 1212–1216.
- [17] Yuan, P.; Schwartz, M. "NMR relaxation study of reorientation and association of acetonitrile in solution". *Spectrochim. Acta A Mol. Spectrosc.* **1992**, *48*, 1523–1527.
- [18] Gerig, J. "Simulations of Nuclear Spin Relaxation in Liquid Acetonitrile". *Mol. Simulat.* **2012**, *38*, 1085–1093.
- [19] Evans, M. "Molecular dynamics and structure of liquid acetonitrile A review and computer simulation". *J. Mol. Liq.* **1983**, *25*, 149–175.
- [20] Westlund, P.-O.; Lynden-Bell, R. "A Molecular Dynamics Study of the Intermolecular Spin-Spin Dipole-dipole Correlation Function of Liquid Acetonitrile". *J. Mag. Res.* **1987**, *72*, 522–531.
- [21] Mammoli, D.; Canet, E.; Buratto, R. "Collisional cross-section of water molecules in vapour studied by means of 1H relaxation in NMR". *Sci Rep* **2016**, *6*, 38492–38492.
- [22] Bloembergen, N.; Purcell, E.; Pound, R. "Relaxation effects in nuclear magnetic resonance absorption". *Phys. Rev.* **1948**, *73*, 679–715.
- [23] Redfield, A. G. "On the Theory of Relaxation Processes". IBM J. Res. Develop. 1957, 1, 19–31.

- [24] Bloch, F. "Nuclear Induction". Phys. Rev. 1946, 70, 460–474.
- [25] Abragam, A. "The Principles of Nuclear Magnetism". Am. J. Phys. 1961, 29, 860.
- [26] Spiess, H. W. Rotation of Molecules and Nuclear Spin Relaxation. In *NMR Basic Principles and Progress*, Vol. 15; P. Diehl, R. K. E. Fluck, Ed.; Springer: Berlin, 1978 55–214.
- [27] Hubbard, P. S. "Nuclear Magnetic Relaxation by Intermolecular Dipole-Dipole Interactions". *Phys. Rev.* **1963**, *131*, 275–282.
- [28] Hardy, W. N. "Nuclear Spin Relaxation in Gaseous H2 at Low Densities". *Can. J. Phys.* **1966**, *44*, 265–280.
- [29] Bloom, M.; Bridges, F.; Hardy, W. N. "Nuclear Spin Relaxation in Gaseous Methane and its Deuterated Modifications". *Can. J. Phys.* **1967**, *45*, 3533–3554.
- [30] Bloom, M.; Dorothy, R. "Determination of the Spin-Rotation Interaction Constants in CH4 by Means of Nuclear Spin Relaxation Measurements". *Can. J. Phys.* **1967**, *45*, 3411–3413.
- [31] Dong, R.; Bloom, M. "Determination of spin-rotation interaction constants in fluorinated methane molecules by means of nuclear spin relaxation measurements". *Can. J. Phys.* **1970**, *48*, 793–804.
- [32] McClung, R. "Rotational Diffusion of Spherical Top Molecules in Liquids". *J. Chem. Phys.* **1969**, *51*, 3842–3852.
- [33] Courtney, J. A.; Armstrong, R. L. "A Nuclear Spin Relaxation Study of the Spin Rotation Interaction in Spherical Top Molecules". *Can. J. Phys.* **1972**, *50*, 1252–1261.
- [34] Armstrong, R. L. "Longitudinal Nuclear Spin Relaxation Time Measurements in Molecular Gases". *13*, **1976**, 71–95.
- [35] Jameson, C. J. "Gas-phase NMR spectroscopy". Chem. Rev. 1991, 91, 1375–1395.
- [36] Jameson, C. J. Gas Phase NMR; The Royal Society of Chemistry: 2016 pp 1–51.
- [37] Engström, S.; Jönsson, B. "Molecular dynamic simulation of quadrupole relaxation of atomic ions in aqueous solution". *J. Chem. Phys.* **1984**, *80*, 5481–5486.
- [38] Roberts, J. E.; Schnitker, J. "Ionic quadrupolar relaxation in aqueous solution: dynamics of the hydration sphere". *J. Phys. Chem.* **1993**, *97*, 5410–5417.
- [39] Chen, S. W.; Rossky, P. J. "Influence of Solvent and Counterion on ²³Na⁺ Spin Relaxation in Aqueous Solution". *J. Phys. Chem.* **1993**, *97*, 10803–10812.

- [40] Luhmer, M.; Reisse, J. "Quadrupole NMR Relaxation of the Noble Gases Dissolved in Simple Liquids and Solutions a Critical Review of Experimental Data in the Light of Computer Simulation Results". *Prog. Nucl. Magn. Reson. Spectrosc.* **1998**, *33*, 57–76.
- [41] Schmidt, J.; Hutter, J.; Spiess, H.-W.; Sebastiani, D. "Beyond Isotropic Tumbling Models: Nuclear Spin Relaxation in Liquids from First Principles". *ChemPhysChem* **2008**, *9*, 2313–2316.
- [42] Carof, A.; Salanne, M.; Charpentier, T.; Rotenberg, B. "On the microscopic fluctuations driving the NMR relaxation of quadrupolar ions in water". *J. Chem. Phys.* **2015**, *143*, 194504.
- [43] Hubbard, P. S. "Theory of Nuclear Magnetic Relaxation by Spin-Rotational Interactions in Liquids". *Phys. Rev.* **1963**, *131*, 1155–1165.
- [44] Aidas, K.; Angeli, C.; Bak, K. L.; Bakken, V.; Bast, R.; Boman, L.; Christiansen, O.; Cimiraglia, R.; Coriani, S.; Dahle, P. et al. "The Dalton quantum chemistry program system". Wiley Interdiscip. Rev. Comput. Mol. Sci. 2014.
- [45] Giannozzi, P.; Baroni, S.; Bonini, N.; Calandra, M.; Car, R.; Cavazzoni, C.; Ceresoli, D.; Chiarotti, G. L.; Cococcioni, M.; Dabo, I. *et al.* "QUANTUM ESPRESSO: a modular and open-source software project for quantum simulations of materials". *J. Phys. Cond. Mat.* **2009**, *21*, 395502.
- [46] Kühne, T. D.; Iannuzzi, M.; Del Ben, M.; Rybkin, V. V.; Seewald, P.; Stein, F.; Laino, T.; Khaliullin, R. Z.; Schütt, O.; Schiffmann, F. *et al.* "CP2K: An electronic structure and molecular dynamics software package Quickstep: Efficient and accurate electronic structure calculations". *J. Chem. Phys.* **2020**, *152*, 194103.
- [47] Grimme, S.; Antony, J.; Ehrlich, S.; Krieg, H. "A consistent and accurate ab initio parametrization of density functional dispersion correction (DFT-D) for the 94 elements H-Pu". *J. Chem. Phys.* **2010**, *132*, 154104.
- [48] TINKER Software Tools for Molecular Design by J. W. Ponder. URL https://dasher.wustl.edu/tinker/. Accessed 08/21,.
- [49] Bussi, G.; Donadio, D.; Parrinello, M. "Canonical sampling through velocity rescaling". *J. Chem. Phys.* **2007**, *126*, 014101.
- [50] Kutzelnigg, W.; Fleischer, U.; Schindler, M. *Deuterium and Shift Calculation. NMR Basic Principles and Progress*, Springer-Verlag: Heidelberg, Germany, **1991**, Vol. 23, pp 165–262.
- [51] Schuchardt, K. L.; Didier, B. T.; Elsethagen, T.; Sun, L.; Gurumoorthi, V.; Chase, J.; Li, J.; Windus, T. L. "Basis Set Exchange: A Community Database for Computational Sciences". *J. Chem. Inf. Model.* **2007**, *47*, 1045–1052.

- [52] Rahman, A.; Stillinger, F. H. "Molecular Dynamics Study of Liquid Water". *J. Chem. Phys.* **1971**, 55, 3336–3359.
- [53] Kowalewski, J.; Mäler, L. *Nuclear spin relaxation in liquids: Theory, experiments, and applications*; Taylor & Francis: New York, 2006.
- [54] Keeler, J. Understanding NMR Spectroscopy; John Wiley & Sons: West Sussex, 2nd ed.; 2010.

TOC Graphic

